Acta Crystallographica Section F
Structural Biology and Crystallization Communications
ISSN 1744-3091

Purification, crystallization and X-ray crystallographic analysis of *Archaeoglobus fulgidus* neelaredoxin

Tiago M. Bandeiras,[a,b]* Célia V. Romão,[a] João V. Rodrigues,[a] Miguel Teixeira[a] and Pedro M. Matias[a]

[a]Instituto de Tecnologia Química e Biológica, Universidade Nova de Lisboa, Apartado 127, 2781-901 Oeiras, Portugal, and [b]Instituto de Biologia Experimental e Tecnológica (IBET), Apartado 12, P-2781-901 Oeiras, Portugal

Correspondence e-mail: tiagob@itqb.unl.pt

Received 20 November 2009
Accepted 7 January 2010

Neelaredoxins are a type of superoxide reductase (SOR), which are blue 14 kDa metalloproteins with a catalytic nonhaem iron centre coordinated by four histidines and one cysteine in the ferrous form. Anaerobic organisms such as *Archaeoglobus fulgidus*, a hyperthermophilic sulfate-reducing archaeon, have developed defence mechanisms against toxic oxygen species in which superoxide reductases play a key role. SOR is responsible for scavenging toxic superoxide anion radicals ($O_2^{\cdot-}$), catalysing the one-electron reduction of superoxide to hydrogen peroxide. Crystals of recombinant *A. fulgidus* neelaredoxin in the oxidized form (13.7 kDa, 125 residues) were obtained using polyethylene glycol and ammonium sulfate. These crystals diffracted to 1.9 Å resolution and belonged to the tetragonal space group $P4_12_12$, with unit-cell parameters $a = b = 75.72$, $c = 185.44$ Å. Cell-content analysis indicated the presence of a tetramer in the asymmetric unit, with a Matthews coefficient (V_M) of 2.36 Å^3 Da^{-1} and an estimated solvent content of 48%. The three-dimensional structure was determined by the MAD method and is currently under refinement.

1. Introduction

Superoxide ($O_2^{\cdot-}$) scavenging enzymes are key antioxidant systems in living organisms as they maintain the concentration of superoxide below poisonous thresholds. This toxic species is formed in cells either continuously in the case of aerobes or transiently in the case of anaerobes and is the product of uncontrolled one-electron reduction of oxygen (Halliwell & Gutteridge, 1999). At present, two types of metal-containing enzymes are known to eliminate $O_2^{\cdot-}$ in an extremely efficient way: superoxide dismutases (SODs) and superoxide reductases (SORs) (Imlay, 2003; Pinto *et al.*, 2009). These enzymes operate using distinct mechanisms; although they share a common step, $O_2^{\cdot-}$ reduction, SOD is also able to catalyze the oxidation of $O_2^{\cdot-}$ whereas SOR is not. The reasons for the different reactivities shown by these enzymes are still unclear.

Superoxide reductases are mononuclear nonhaem iron proteins and are classified according to the number of iron centres as 1Fe-SORs (neelaredoxins) or 2Fe-SORs (desulfoferrodoxins) (see, for example, Pinto *et al.*, 2009). In addition to the iron centre of the active site, 2Fe-SORs possess a second N-terminal protein domain with a desulforedoxin fold containing an additional iron centre $[Fe(Cys)_4]^{3+}$, the function of which is still unknown. The common iron centre responsible for $O_2^{\cdot-}$ reduction is pentacoordinated in the ferrous state, with the imidazole N atoms of four equatorial histidine ligands and one axial cysteine ligand in a square pyramidal-like geometry $[Fe(Cys)(His)_4]$ (Yeh *et al.*, 2000; Santos-Silva *et al.*, 2006; Coelho *et al.*, 1997; Adam *et al.*, 2004). In the SOR resting state, when the protein is fully oxidized, a sixth glutamate ligand is present at the other axial position, yielding an octahedrally coordinated metal centre (Yeh *et al.*, 2000; Adams *et al.*, 2002; Berthomieu *et al.*, 2002).

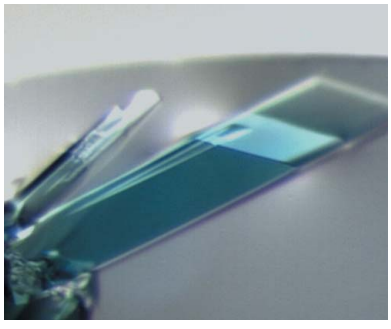

However, it should be noticed that this glutamate is not strictly conserved among SORs (Pinto *et al.*, 2009).

The superoxide-reduction mechanisms of the different SOR families have been studied by pulse radiolysis and stopped-flow spectrometry, and it seems clear that SORs from different sources show striking differences in their kinetics upon reaction with O_2^- (Nivière *et al.*, 2004; Emerson *et al.*, 2003; Rodrigues *et al.*, 2006, 2007, 2008). It has previously been shown that both 1Fe-SOR and 2Fe-SOR from the hyperthermophilic archaeon *Archaeoglobus fulgidus* react with O_2^- at diffusion-limited rates of $\sim 10^9\ M^{-1}\ s^{-1}$ to form an Fe^{3+}-(hydro)peroxide transient that decays to an intermediate in which a solvent molecule is initially bound to the iron and is then displaced by a glutamate residue (Rodrigues *et al.*, 2006, 2007). In contrast, although a similar Fe^{3+}-(hydro)peroxide transient is formed in the case of the 2Fe-SOR from the mesophile *Desulfovibrio vulgaris*, in this enzyme this intermediate decays directly to the final Fe^{3+}-glutamate resting state (Emerson *et al.*, 2003; Huang *et al.*, 2007).

Crystal structures have been solved of 2Fe-SORs from the bacteria *Desulfovibrio desulfuricans* (Coelho *et al.*, 1997) and *Desulfoarculus baarsii* (Adam *et al.*, 2004) and of 1Fe-SORs from the archaea *Pyrococcus furiosus* (Yeh *et al.*, 2000) and *P. horikoshii* and the bacteria *Thermotoga maritima* and *Treponema pallidum* (Santos-Silva *et al.*, 2006); the *T. pallidum* enzyme has an additional N-terminal domain but lacks the second iron centre [$Fe(Cys)_4$]. All these SOR molecules from different sources present similar architectural folds; the oligomerization states (homodimers or tetramers) appear to be correlated with the absence or presence of the extra N-terminal domain, respectively.

The superoxide reductase isolated from *A. fulgidus*, a hyperthermophilic sulfate-reducing archaeon, was isolated as a functional homotetramer of four 14 kDa subunits (Abreu *et al.*, 2000). The crystal structure of *A. fulgidus* SOR will be the second crystal structure of a 1Fe-SOR, also known as neelaredoxin (Nlr), from an archaeon and the first example of a fully oxidized 1Fe-SOR. Comparison with known three-dimensional SOR structures, together with detailed analysis of the iron active site, will contribute to clarification of the remaining questions regarding the superoxide-reduction mechanism.

2. Experimental procedures and results

2.1. Protein expression and purification

The overexpression and purification of *A. fulgidus* neelaredoxin (*Af* Nlr) were performed as described previously (Rodrigues *et al.*, 2006) with some modifications. For the overexpression of *A. fulgidus* neelaredoxin, cultures of BL21-Gold (DE3) cells (Stratagene) containing the plasmid pT7AfNlr (Abreu *et al.*, 2000) were grown aerobically at 303 K in M9 minimal medium supplemented with 100 µg ml^{-1} ampicillin and 100 µ*M* $FeSO_4$ in a 10 l fermenter. When the culture reached a cell density of A_{600} = 0.3, 0.1 m*M* isopropyl *β*-D-1-thiogalactopyranoside was added and after 6 h induction the cells were harvested by centrifugation (10 000*g*, 10 min) and washed with 10 m*M* Tris–HCl pH 7.6. All subsequent purification steps were performed at 277 K. The cells were broken in a mini-cell French press at 6.2 MPa and the soluble fraction was obtained by ultracentrifugation (100 000*g*, 4 h). After overnight dialysis against 10 m*M* Tris–HCl pH 7.6, the sample was degassed and incubated for ∼1 h at 277 K with 1 m*M* dithiothreitol, 10 m*M* ascorbate and 0.1 m*M* $FeSO_4$ under anaerobic conditions by purging with N_2. The sample was then loaded onto a Q-Sepharose column (Pharmacia) previously equilibrated with Tris–HCl pH 7.6. A linear gradient of 0–0.5 *M* NaCl was applied and the fraction containing *Af* Nlr was eluted at 0.25 *M* NaCl. This fraction was dialyzed against 10 m*M* Tris–HCl pH 7.6 and loaded onto a Fractogel EMD TMAE column (Merck) equilibrated with the same buffer. A linear gradient of 0–0.5 *M* NaCl was applied and the fraction containing *Af* Nlr was eluted at 0.25 *M* NaCl. The sample was concentrated by ultrafiltration (Millipore) and loaded onto a Superdex 200 column (Pharmacia) equilibrated with 20 m*M* Tris–HCl pH 7.6 and 150 m*M* NaCl. This last step allows effective separation of the most abundant tetrameric form of neelaredoxin from other higher oligomeric states of the protein, as described by Rodrigues *et al.* (2006). Protein purity was tested by SDS–PAGE (Fig. 1) and the Bicinchoninic Acid Protein Assay Kit (Pierce; Smith *et al.*, 1985) was used to determine the protein concentration. The total iron content was determined using the 2,4,6-tripyridyl-*s*-triazine (TPTZ) method (Fisher & Price, 1964). The oxidized protein was prepared by incubation with a slight excess of K_2IrCl_6 and the oxidant was removed by repeated dilutions and concentrations in a Centricon device.

2.2. Crystallization and cryoprotection

Preliminary crystallization trials were performed with protein concentrated to 15 mg ml^{-1} in 20 m*M* phosphate buffer pH 7.5, 150 m*M* NaCl using the vapour-diffusion technique. Nanolitre-scale drops were prepared with the commercially available Classics I kit (Qiagen) using a Cartesian Crystallization Robot Dispensing System (Genomics Solutions) with round-bottom 96-well Greiner CrystalQuick plates (Greiner Bio-One). Three different drop proportions were prepared per condition screened, using (i) 100 nl reservoir solution and 100 nl protein solution, (ii) 100 nl reservoir solution and 200 nl protein solution and (iii) 200 nl reservoir solution and 100 nl protein solution. The drops were equilibrated against 100 µl reservoir solution. Blue crystalline forms were observed using condition No. 85 of the Classics I screen, consisting of 0.2 *M* ammonium sulfate, 0.1 *M* sodium acetate pH 4.6 and 25% polyethylene glycol (PEG) 4000. Additional optimization experiments were carried out in order to improve the crystal quality and size. Different modifications of the initial condition were tested using the sitting-drop vapour-diffusion method at 277, 293 and 303 K in 24-well crystallization plates. The best crystals were grown after 2–3 d by mixing 1.5 µl reservoir solu-

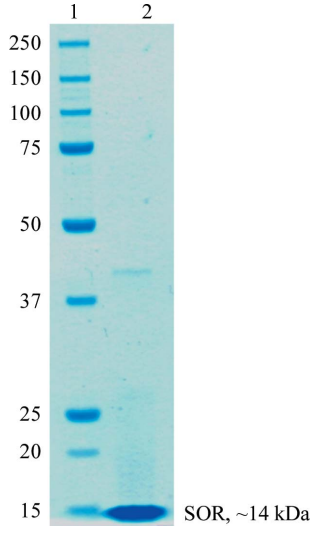

Figure 1
10% SDS–PAGE gel of pure recombinant *Af* Nlr. Lane 1, Bio-Rad unstained protein markers (product No. 161-0363). Lane 2, *Af* Nlr monomer migrating according to a molecular mass of 13.7 kDa.

tion containing 0.2 *M* ammonium sulfate, 0.1 *M* sodium acetate pH 4.6, 15% PEG 4000 with 1.5 µl protein solution and equilibrating against 500 µl reservoir solution. Quadrangular prismatic blue crystals grew for 10 d and reached final dimensions of 0.3–2 mm in the longest axis (Fig. 2). *Af* Nlr crystals were cryoprotected using reservoir solution supplemented with 25% glycerol prior to flash-cooling in liquid nitrogen.

2.3. Data collection and crystallographic analysis

The vast majority of the *Af* Nlr crystals tested for X-ray diffraction were highly anisotropic and their diffraction images could not be indexed. However, the diffraction pattern of one *Af* SOR crystal could be indexed and a three-wavelength MAD data set was collected at 100 K from this crystal using a MAR 225 CCD detector on the tunable-wavelength beamline BM14 at ESRF, Grenoble. An X-ray fluorescence spectrum near the Fe *K* absorption edge was measured in order to select the monochromator settings for the peak (λ_1 = 1.740 Å, maximum $\Delta f''$) and the inflection-point (λ_2 = 1.741 Å, minimum $\Delta f'$) wavelengths using *CHOOCH* (Evans & Pettifer, 2001). The high-energy remote wavelength λ_3 was chosen as 0.9537 Å.

All data sets were integrated with *MOSFLM* (Leslie, 1992) and scaled with *SCALA* from the *CCP*4 suite (Collaborative Computational Project, Number 4, 1994). The data-collection and processing statistics are summarized in Table 1. The *Af* Nlr crystal belonged to one of the enantiomorphic tetragonal space groups $P4_12_12$ or $P4_32_12$, with unit-cell parameters $a = b = 75.72$, $c = 185.44$ Å. The Matthews coefficient was determined as $V_M = 2.36$ Å^3 Da^{-1}, suggesting the presence of four SOR molecules in the asymmetric unit with a predicted solvent content of 48%.

2.4. Structure determination

The three-dimensional structure of *Af* Nlr was solved using the MAD method. Matthews coefficient calculations suggested the presence of one Nlr tetramer in the asymmetric unit, hence four Fe sites were expected. Using the *HKL2MAP* graphical user interface (Pape & Schneider, 2004), the MAD data set was analysed with *SHELXC*, the heavy-atom substructure was determined with *SHELXD* and the phase problem was solved with *SHELXE* (Sheldrick, 2008). *SHELXD* found at least one possible solution out of 200 trials, the best of which had a correlation coefficient of 51.36% and contained four possible iron sites in the crystal asymmetric unit with occupancy factors ranging from 0.85 to 1.0. *SHELXE* gave a clear discrimination between the correct and inverted substructures and resolved the space-group ambiguity in favour of $P4_12_12$.

Automated model building was performed with *Buccaneer* (Cowtan, 2006) using the 1.9 Å remote-wavelength data set, which generated a complete 500-residue model with R = 0.361 and R_{free} = 0.381 and a mean figure of merit of 0.642. R_{free} was based on a randomly chosen 5% subset of the measured data. The Fe atoms in the SOR active sites were modelled using *Coot* (Emsley & Cowtan, 2004) and the structure is currently under refinement.

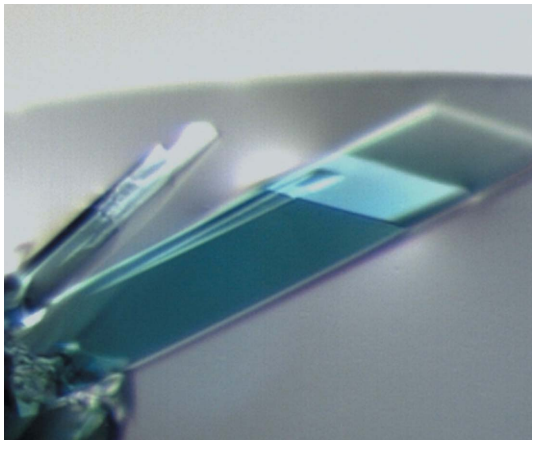

Figure 2
Crystals of *A. fulgidus* superoxide reductase (neelaredoxin) grown in 0.2 *M* ammonium sulfate, 0.1 *M* sodium acetate pH 4.6, 15%(*v*/*v*) PEG 4000. The crystal dimensions are ~0.6 × 0.2 × 0.15 mm.

Table 1
Data-collection and processing statistics.

Values in parentheses are for the last resolution shell.

	Peak	Inflection	Remote
Wavelength (Å)	1.740	1.741	0.9537
Resolution range (Å)	46.4–2.4 (2.5–2.4)	46.4–2.2 (2.3–2.2)	37.1–1.9 (2.0–1.9)
Completeness, overall (%)	100 (100)	99.9 (99.5)	100 (100)
Completeness, anomalous (%)	100 (100)	99.9 (99.1)	100 (99.9)
No. of observations	156599 (22337)	190247 (21348)	297205 (36951)
No. of unique reflections	22579 (3219)	28388 (4020)	42230 (6054)
Multiplicity, overall	6.9 (6.9)	6.7 (5.3)	7.0 (6.1)
Multiplicity, anomalous	3.6 (3.5)	3.5 (2.7)	3.6 (3.0)
R_{merge}† (%)	0.071 (0.270)	0.065 (0.318)	0.071 (0.364)
R_{anom} (%)	0.047 (0.122)	0.036 (0.167)	0.028 (0.176)
$R_{p.i.m.}$‡ (%)	0.042 (0.166)	0.039 (0.220)	0.042 (0.238)
$\langle I/\sigma(I)\rangle$	6.3 (1.9)	8.2 (2.0)	7.2 (2.0)

† $R_{merge} = \sum_{hkl}\sum_i |I_i(hkl) - \langle I(hkl)\rangle| / \sum_{hkl}\sum_i I_i(hkl)$. ‡ $R_{p.i.m.} = \sum_{hkl}[1/(N-1)]^{1/2} \sum_i |I_i(hkl) - \langle I(hkl)\rangle| / \sum_{hkl}\sum_i I_i(hkl)$, where $I_i(hkl)$ is the observed intensity, $\langle I(hkl)\rangle$ is the average intensity of multiple observations from symmetry-related reflections and N is their redundancy.

The authors would like to acknowledge José A. Brito for assistance with data processing and phasing at ITQB. JR is the recipient of an FCT-MCTES (Portugal) fellowship (SFRH/BPD/34763/2007). The work was supported by Fundação para a Ciência e Tecnologia Project PTDC/BIA-PRO/67263/2006. We would like to thank the EMBL Grenoble Outstation for providing support for measurements on the ESRF EMBL–CRG BM14 beamline under the European Community Access to Research Infrastructure Action FP6 Programme 'Structuring the European Research Area Specific Program' with contract No. RII3-CT-2004-506008. The help and advice given by Martin A. Walsh and Hassan Belrhali (EMBL, Grenoble) during the BM14 data collections is also gratefully acknowledged.

References

Abreu, I. A., Saraiva, L. M., Carita, J., Huber, H., Stetter, K. O., Cabelli, D. & Teixeira, M. (2000). *Mol. Microbiol.* **38**, 322–334.
Adam, V., Royant, A., Nivière, V., Molina-Heredia, F. P. & Bourgeois, D. (2004). *Structure*, **12**, 1729–1740.
Adams, M. W., Jenney, F. E. Jr, Clay, M. D. & Johnson, M. K. (2002). *J. Biol. Inorg. Chem.* **7**, 647–652.
Berthomieu, C., Dupeyrat, F., Fontecave, M., Verméglio, A. & Nivière, V. (2002). *Biochemistry*, **41**, 10360–10368.
Coelho, A. V., Matias, P., Fülöp, V., Thompson, A., Gonzalez, A. & Carrondo, M. A. (1997). *J. Biol. Inorg. Chem.* **2**, 680–689.
Collaborative Computational Project, Number 4 (1994). *Acta Cryst.* D**50**, 760–763.
Cowtan, K. (2006). *Acta Cryst.* D**62**, 1002–1011.
Emerson, J. P., Cabelli, D. E. & Kurtz, D. M. Jr (2003). *Proc. Natl Acad. Sci. USA*, **100**, 3802–3807.
Emsley, P. & Cowtan, K. (2004). *Acta Cryst.* D**60**, 2126–2132.
Evans, G. & Pettifer, R. F. (2001). *J. Appl. Cryst.* **34**, 82–86.
Fisher, D. S. & Price, D. C. (1964). *Clin. Chem.* **10**, 21–31.

Halliwell, B. & Gutteridge, J. M. C. (1999). *Free Radicals in Biology and Medicine*, 3rd ed. Oxford University Press.
Huang, V. W., Emerson, J. P. & Kurtz, D. M. Jr (2007). *Biochemistry*, **46**, 11342–11351.
Imlay, J. A. (2003). *Annu. Rev. Microbiol.* **57**, 395–418.
Leslie, A. G. W. (1992). *Jnt CCP4/ESF–EACBM Newsl. Protein Crystallogr.* **26**.
Nivière, V., Asso, M., Weill, C. O., Lombard, M., Guigliarelli, B., Favaudon, V. & Houée-Levin, C. (2004). *Biochemistry*, **43**, 808–818.
Pape, T. & Schneider, T. R. (2004). *J. Appl. Cryst.* **37**, 843–844.
Pinto, A. F., Rodrigues, J. V. & Teixeira, M. (2009). *Biochim. Biophys. Acta*, doi:10.1016/j.bbapap.2009.10.011.
Rodrigues, J. V., Abreu, I. A., Cabelli, D. & Teixeira, M. (2006). *Biochemistry*, **45**, 9266–9278.
Rodrigues, J. V., Saraiva, L. M., Abreu, I. A., Teixeira, M. & Cabelli, D. E. (2007). *J. Biol. Inorg. Chem.* **12**, 248–256.
Rodrigues, J. V., Victor, B. L., Huber, H., Saraiva, L. M., Soares, C. M., Cabelli, D. E. & Teixeira, M. (2008). *J. Biol. Inorg. Chem.* **13**, 219–228.
Santos-Silva, T., Trincão, J., Carvalho, A. L., Bonifácio, C., Auchère, F., Raleiras, P., Moura, I., Moura, J. J. G. & Romão, M. J. (2006). *J. Biol. Inorg. Chem.* **11**, 548–558.
Sheldrick, G. M. (2008). *Acta Cryst.* A**64**, 112–122.
Smith, P. K., Krohn, R. I., Hermanson, G. T., Mallia, A. K., Gartner, F. H., Provenzano, M. D., Fujimoto, E. K., Goeke, N. M., Olson, B. J. & Klenk, D. C. (1985). *Anal. Biochem.* **150**, 76–85.
Yeh, A. P., Hu, Y., Jenney, F. E. Jr, Adams, M. W. & Rees, D. C. (2000). *Biochemistry*, **39**, 2499–2508.